

RESEARCH PAPER

# Hydrothermal Preparation of Cobalt, Nickel, Copper Ferrite Nanoparticles and Study of Microhardness of Aluminum-based Nanocomposites

Mohsen Hosseini<sup>1</sup>, Hamidreza Rezaei Ashtiani<sup>1\*</sup>, Davood Ghanbari<sup>2</sup>

<sup>1</sup> School of Mechanical Engineering, Arak University of Technology, Arak, Iran

<sup>2</sup> Department of Science, Arak University of Technology, Arak, Iran

## ARTICLE INFO

### Article History:

Received 20 December 2020

Accepted 18 March 2021

Published 01 April 2021

### Keywords:

Friction stir processing

Hydrothermal

Nanocomposite

Nanoparticles

## ABSTRACT

In this paper, first different ferrite nanoparticles including,  $\text{CoFe}_2\text{O}_4$ ,  $\text{NiFe}_2\text{O}_4$ , and  $\text{CuFe}_2\text{O}_4$  were synthesized using the hydrothermal method, then for investigation of the properties, various analyzes including SEM, XRD, and VSM were taken from them. Then using the friction stir processing technique, these nanoparticles were poured into AA7075 aluminum alloy and a surface composite was created. Results showed that all particles are in nanoscale and have a uniform and fine-grained structure. Also, the micro-hardness of the produced nanocomposites was significantly increased.

## How to cite this article

Hosseini M, Rezaei Ashtiani H, and Ghanbari D. Hydrothermal Preparation of Cobalt, Nickel, Copper Ferrite Nanoparticles and Study of Microhardness of Aluminum-based Nanocomposites. J Nanostruct, 2021; 11(2): 409-417 DOI: 10.22052/JNS.2021.02.020

## INTRODUCTION

There are various methods for making nanoparticles, one of them is hydrothermal, which is widely used today due to its mild operation parameters [1] and better controllable particle size [2, 3]. In addition to hydrothermal, the synthesis is one-step without the need for sintering and calcination [4]. Also low cost, able to control the shape, size, and phase, and low energy consumption are other features of this method [5-8]. This method is an easy and eco-friendly method that is used to prepare various nanostructures such as nanospheres, nanowires and nanorods [9-12]. Kurian et al. [13] synthesized  $\text{ZnFe}_2\text{O}_4$ ,  $\text{MgFe}_2\text{O}_4$ ,  $\text{CuFe}_2\text{O}_4$  using the hydrothermal method. They observed a cubical and porous spherical morphology for the hydrothermal method. The two main absorption bands in the

FTIR spectrum confirmed the spinel structure of the prepared ferrites. Also porous spherical  $\text{MgFe}_2\text{O}_4$ ,  $\text{ZnFe}_2\text{O}_4$  nanoparticles showed more ferromagnetic properties than cubical particles. Rathinavel et al. [14-19] synthesized magnesium ferrite using the hydrothermal method, and their results confirmed the spinel structure and crystal size of about 29 nm. Ansari et al.<sup>[20]</sup> investigated the magnetic properties of cobalt ferrite synthesized by hydrothermal method as an eco-friendly method. Their results showed that the hydrothermal method can be used as an eco-friendly and economical method for the synthesis of magnetic and super magnetic nanostructured materials at relatively low temperatures. Using the hydrothermal method, Zhang et al. [21] synthesized cobalt ferrite and ZnS nanoparticles

\* Corresponding Author Email: [hr\\_rezaei@arakut.ac.ir](mailto:hr_rezaei@arakut.ac.ir)



to absorb electromagnetic waves and observed particle sizes between 10 to 20 nm with a uniform structure. Also, the wave absorption properties of ferrite composite were improved compared to cobalt ferrite. Malinowska et al [22] synthesized cobalt ferrite nanoparticles and studied their morphology and magnetic properties. The  $\text{CoFe}_2\text{O}_4$  particles from metal sulfate precursors showed the highest saturation magnetization and the lowest coercivity. Also, the average particle size increased from 46 nm to 54 nm with increasing metal concentration and ion resistance. Kurian et al. [23] synthesized  $\text{CoFe}_2\text{O}_4$  nanoparticles using the hydrothermal method. They observed that the time and temperature of the hydrothermal reaction had little effect on the structural and magnetic parameters of the material, although pH played an important role in the physical properties of the nanoparticles. Prabhu et al [24] FSP the 6082 aluminum sheet and investigated its mechanical properties and found that after three FSP passes, the microhardness of the composites improved. Mazaheri et al. [25] produced A356/ $\text{Al}_2\text{O}_3$  nanocomposite using FSP. Their results showed that with uniform distribution of alumina particles, the micro-hardness of the samples is improved. Zayed et al. [26] made the composite using the FSP technique and 5083 aluminum alloy. They mixed Sic and  $\text{Al}_2\text{O}_3$  particles together and added them to the AA5083. The micro-hardness of

the samples increased significantly, and their wear properties also improved.

In this paper first,  $\text{CoFe}_2\text{O}_4$ ,  $\text{NiFe}_2\text{O}_4$ , and  $\text{CuFe}_2\text{O}_4$  nanoparticles were made using the hydrothermal method, and then the surface nanocomposite was produced with AA7075 aluminum alloy as base metal using FSP and its surface properties were investigated.

### MATERIALS AND METHODS

To produce nanoparticles, 0.3 g of  $\text{NiSO}_4$  and 0.92 g of iron nitrate in 150 ml of distilled water were mixed for 30 minutes with a stirrer, and then NaOH 1 molar solution was slowly added to the base solution to bring the pH to 11. Then, the solution is poured into a special hydrothermal vessel and kept at 200 degrees for 4 hours. After this time, the solution is centrifuged and placed in an oven to dry. The same process is repeated to make other nanoparticles, except that 0.97 g of iron nitrate is added for 0.3 g of  $\text{CoSO}_4$  and 1.2 g of iron nitrate is added for 0.3 g of  $\text{CuSO}_4$ . Fig. 1 shows a schematic of the hydrothermal method.

For FSP, 7075 aluminum sheet was used. After the sheet was cut to the appropriate dimensions and prepared and placed inside the fixture, a groove was made on the surface of the sheet with a depth of 2.5 mm and a width of 0.5 mm, and the inside of the groove was filled with the produced nanoparticles. In the next step, the FSP tool which

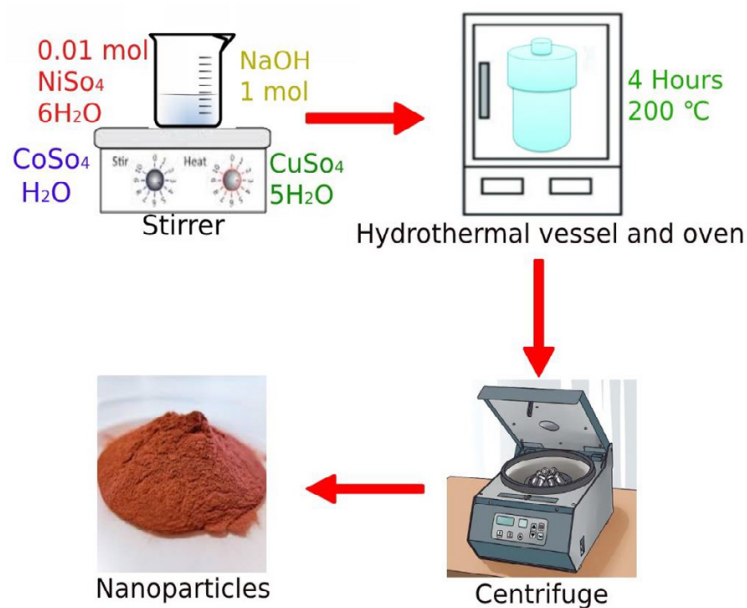


Fig. 1. Schematically fabrication of ferrite nanoparticles by the hydrothermal method

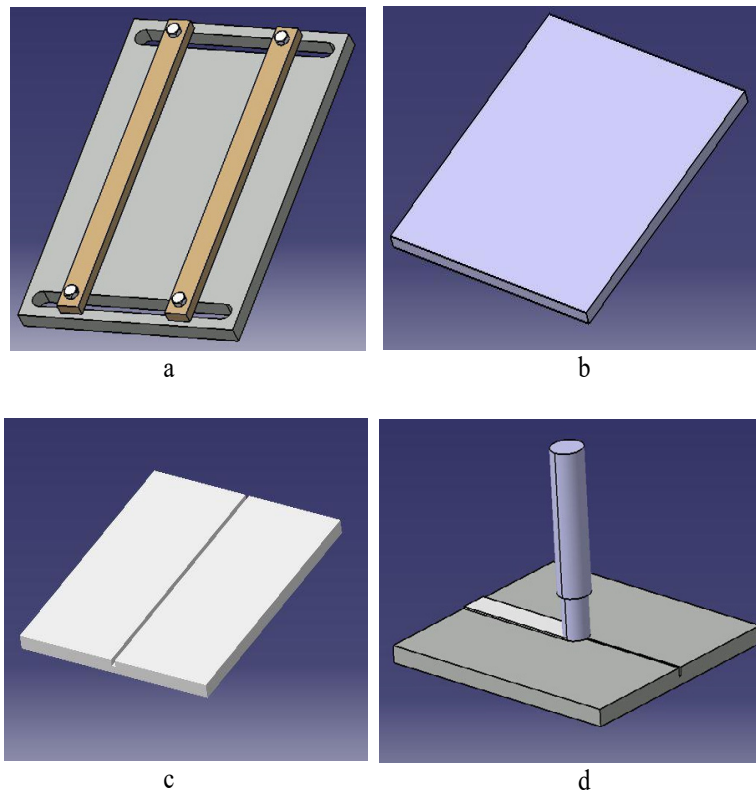


Fig. 2. Schematic of FSP consist of (a) designed fixture, (b) aluminum sheet (c) the groove created on the sheet, and (d) the tool of friction stir processing.

is made of H13 and has a pin with a diameter of 3 mm and a height of 3 mm and a shoulder with a diameter of 14 mm, performed the FSP operation

and surface nanocomposites were created. Rotational and travel speeds of 1200 rpm and 32mm / min were selected, respectively. Then

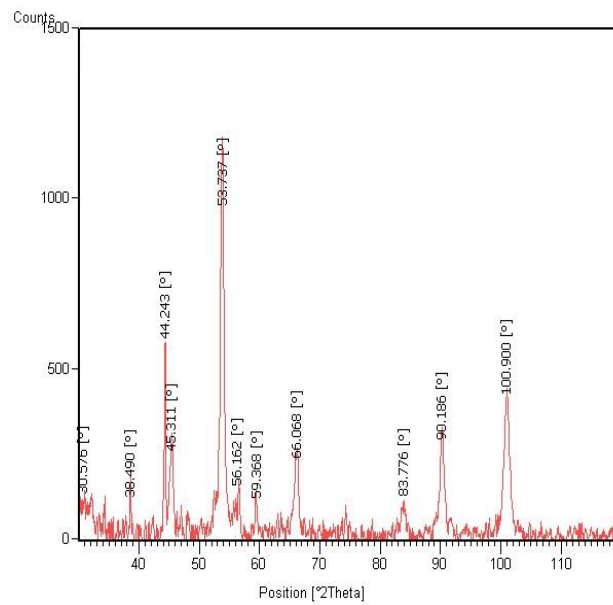


Fig. 3. XRD pattern of  $\text{CoFe}_2\text{O}_4$  nanoparticles.

the samples were cut and prepared for microhardness testing. Microhardness tests were taken from the cross-section of the samples according to standard ASTM E92. The schematic of the friction stir processing is shown in Fig. 2.

**RESULTS AND DISCUSSION**

Fig. 3 shows the XRD pattern of cobalt ferrite nanoparticles ( $\text{CoFe}_2\text{O}_4$ ), this spectrum has appropriate accordance with pure cobalt ferrite

standard using JCPDS: 22-1086 and miller indexes: (111), (220), (311), (222), (400), (422), (511) and (440).

Fig. 4 illustrates the X-ray diffraction pattern (XRD) of nickel ferrite ( $\text{NiFe}_2\text{O}_4$ ) nanoparticles, the pattern has a suitable agreement with pure material standard using JCPDS: 86-2267 and Miller indexes include (111), (220), (311), (222), (400), (422), (511), (440), (533), (622), (444) are observed in the pattern and approve purity of the

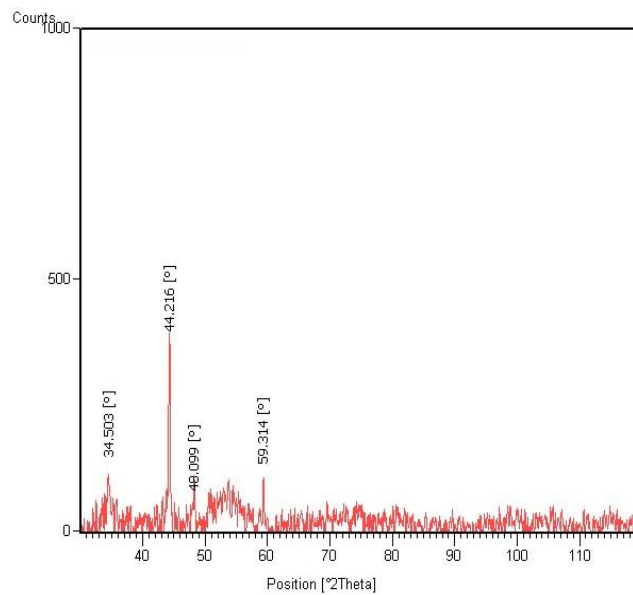


Fig. 4. XRD pattern of the synthesized  $\text{NiFe}_2\text{O}_4$  nanoparticles

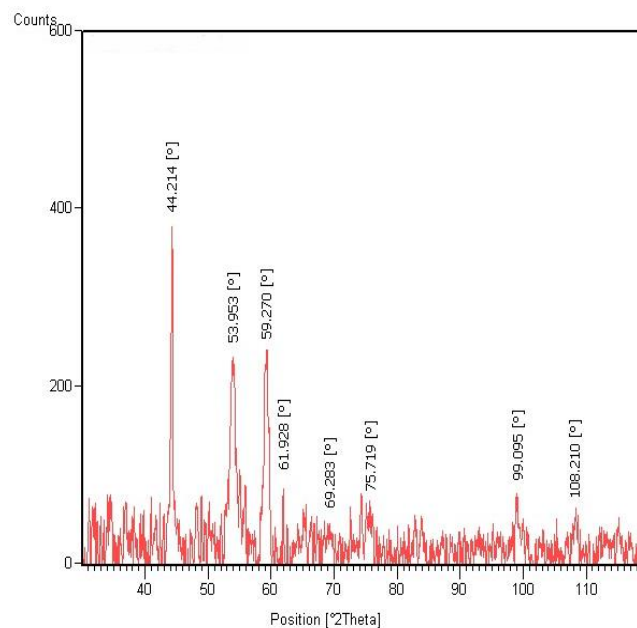


Fig. 5. XRD pattern of  $\text{CuFe}_2\text{O}_4$  nanoparticles

phase in this reaction.

Fig. 5 depicts the XRD pattern of copper ferrite nanoparticle ( $\text{CuFe}_2\text{O}_4$ ) with JCPDS: 34-0425 and by miller indexes: (220), (313), (320), (400), (422), (511), (440).

The Crystallite size of all three fabricated ferrites nanoparticles is measured using the Debye-Sherrer equation, the results show that cobalt, nickel, and copper ferrites nanoparticles have

diameter values of 10, 12, and 15 nm, respectively.

Fig. 6 show scanning electron microscope images, as can be seen in the images, the nanoparticles are well distributed and the particle size is 50-80 nm for cobalt ferrite nanoparticles.

SEM images for nickel ferrite nanoparticles are shown in Fig. 7, mono-disperse and uniform structure with a grain size between 40-70 nm is obtained after the synthesis of nanoparticles.

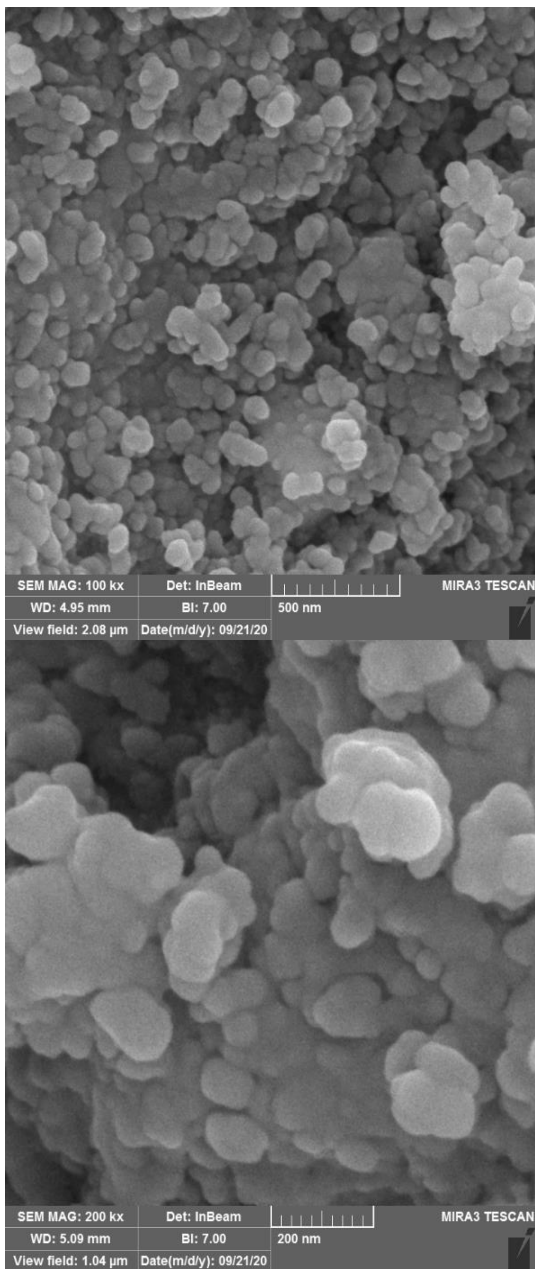


Fig. 6. SEM images of  $\text{CoFe}_2\text{O}_4$  nanoparticles synthesized by hydrothermal method

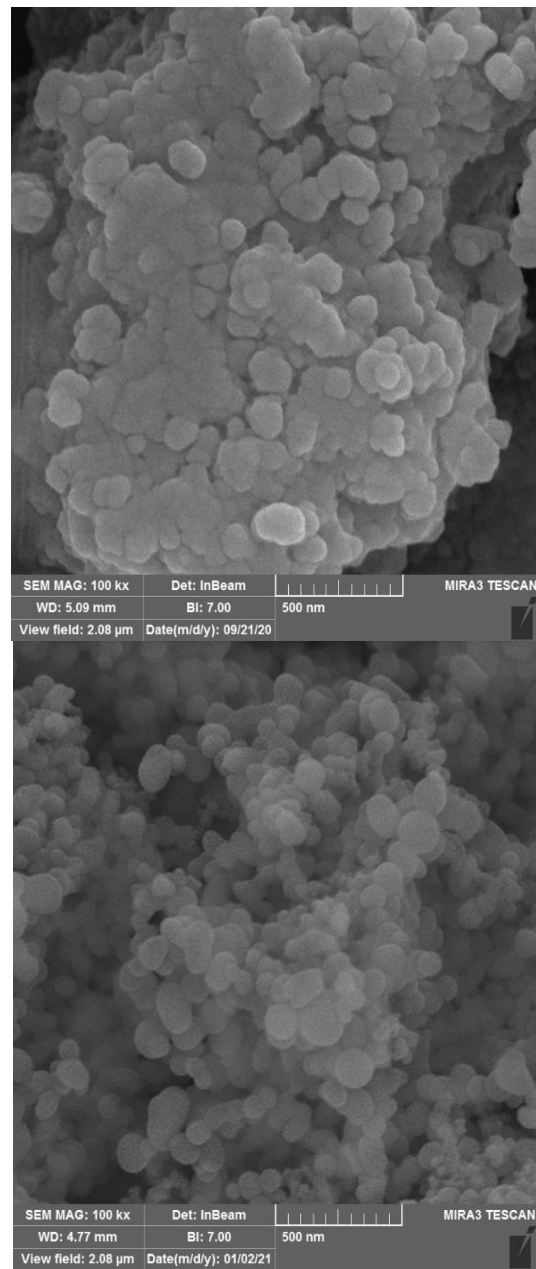


Fig 7. SEM images of  $\text{NiFe}_2\text{O}_4$  nanoparticles prepared by hydrothermal method

Fig. 8 shows SEM images of copper ferrite nanoparticles and the size of the nanoparticles are between 40-70 nanometers. As all samples show despite suitable magnetic property all nanoparticles were prepared at uniform and monodisperse size.

Figs. 9, 10 illustrate vibrating sample

magnetometer (VSM) curves of the three magnetic ferrites consist of cobalt, nickel, and copper ferrites, respectively. VSM loops depict nearly ferromagnetic effects for all three samples of cobalt, nickel, and copper ferrites have saturation magnetization values around 25, 30, and 11 emu/g, respectively. According to these figures,

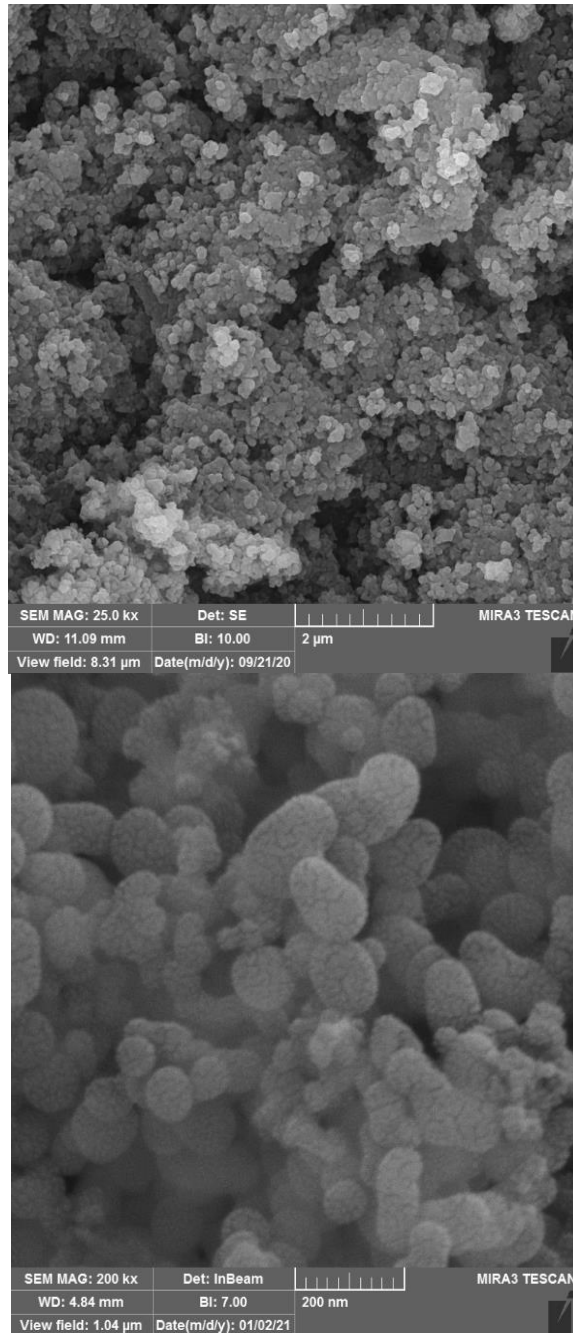


Fig. 8. SEM images of CuFe<sub>2</sub>O<sub>4</sub> nanoparticles produced by hydrothermal method.

magnetization remanence values of cobalt, nickel, and copper ferrites are about 5, 6, and 3 emu/g, respectively. Also, coercivities values are around 130, 200, and 400 Oersted for cobalt, nickel, and copper ferrites nanoparticles, respectively.

Fig. 11 shows the results of the micro-hardness tests. As can be seen, the microhardness values increase as it approaches the center of the stir zone, the higher the microhardness due to the

presence of more nanoparticles and their uniform distribution. However, by moving away from the center part of the stir zone, the microhardness values decrease due to the reduction in the volume of nanoparticles.

It is clear that the maximum microhardness value of FSPed AA7075 and AA7075/CuFe<sub>2</sub>O<sub>4</sub>, AA7075/NiFe<sub>2</sub>O<sub>4</sub>, and AA7075/CoFe<sub>2</sub>O<sub>4</sub> surface nanocomposites have the highest values as in

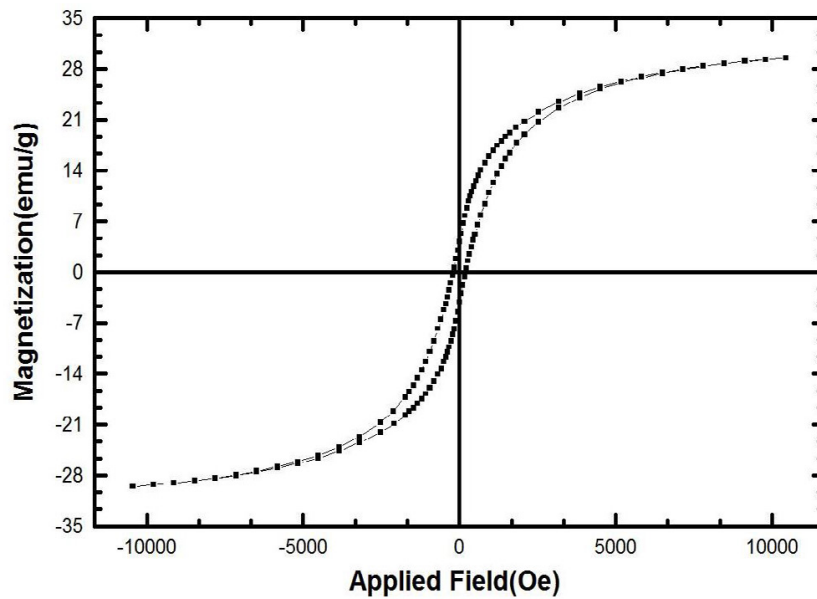


Fig. 9. VSM of the magnetic nickel ferrite nanoparticles.

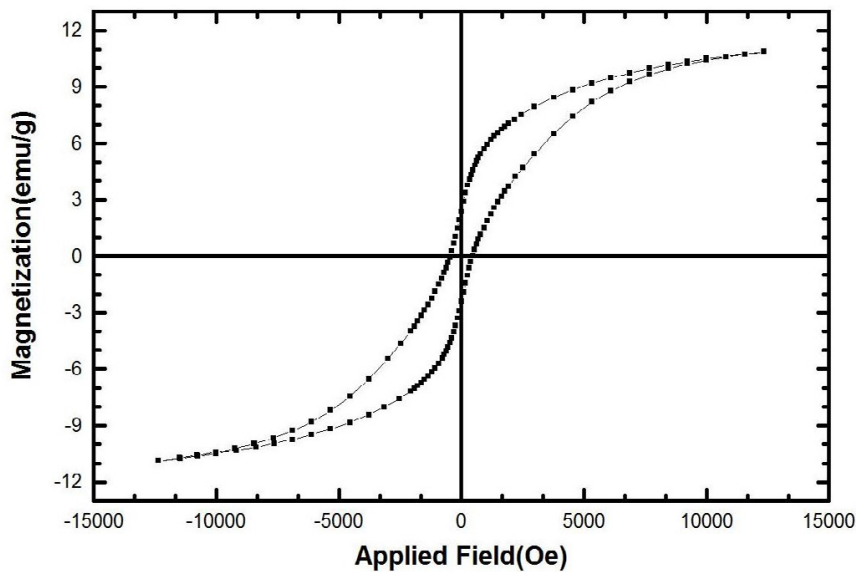


Fig. 10. VSM curve of the magnetic copper ferrite nanoparticles.

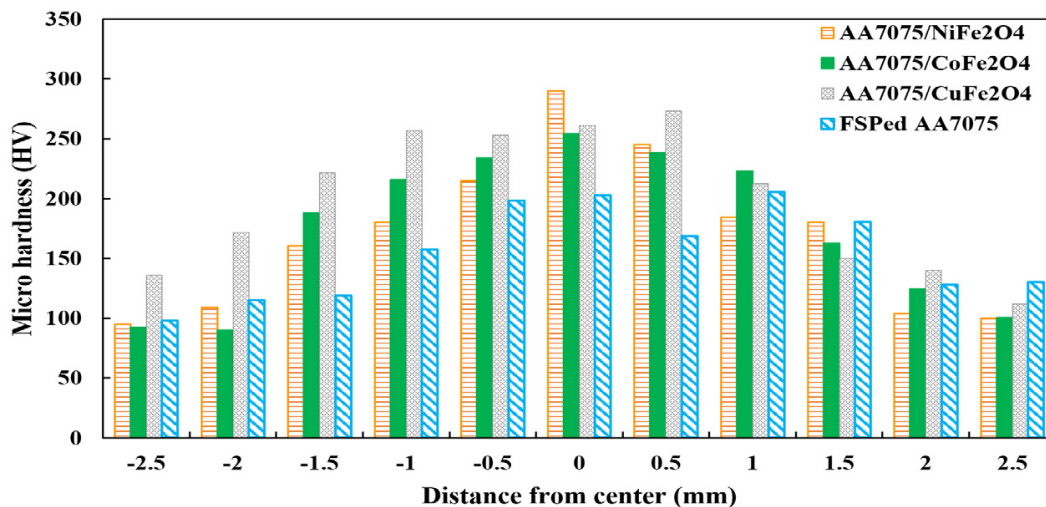


Fig. 11. Comparing of microhardness of the different surface ferritic nanocomposite samples with various nanoparticles and FSP samples.

ascending order.

## CONCLUSION

In this paper, different ferrite nanoparticles were first synthesized in an easy and cost-effective method and their properties were investigated. Then surface nanocomposites were fabricated with these nanoparticles using FSP and their microhardness properties were investigated. Based on the results of this paper, hydrothermal was a suitable method for the production of nanoparticles with a uniform and fine-grained structure, and the fabricated nanoparticles comply with standard peaks. These nanoparticles also have magnetic properties that can be used for radar wave absorption applications. In addition, the fabricated nanoparticles can also improve the mechanical property of the hardness of the surface nanocomposites.

## CONFLICT OF INTEREST

The authors declare that there is no conflict of interests regarding the publication of this manuscript.

## REFERENCES

1. Byrappa K, Adschiri T. Hydrothermal technology for nanotechnology. *Progress in Crystal Growth and Characterization of Materials*. 2007;53(2):117-66.
2. Yao C, Shin Y, Wang L-Q, Windisch CF, Samuels WD, Arey BW, et al. Hydrothermal Dehydration of Aqueous Fructose Solutions in a Closed System. *The Journal of Physical Chemistry C*. 2007;111(42):15141-5.
3. Baccile N, Laurent G, Babonneau F, Fayon F, Titirici M-M,

- Antoniotti M. Structural Characterization of Hydrothermal Carbon Spheres by Advanced Solid-State MAS 13C NMR Investigations. *The Journal of Physical Chemistry C*. 2009;113(22):9644-54.
4. Intaphong P, Phuruangrat A, Karthik K, Dumrongrojthanath P, Thongtem T, Thongtem S. Effect of pH on Phase, Morphology and Photocatalytic Properties of BiOBr Synthesized by Hydrothermal Method. *Journal of Inorganic and Organometallic Polymers and Materials*. 2019;30(3):714-21.
5. Köseoğlu Y, Alan F, Tan M, Yilgin R, Öztürk M. Low temperature hydrothermal synthesis and characterization of Mn doped cobalt ferrite nanoparticles. *Ceramics International*. 2012;38(5):3625-34.
6. Phuruangrat A, Ham DJ, Hong SJ, Thongtem S, Lee JS. Synthesis of hexagonal WO<sub>3</sub>nanowires by microwave-assisted hydrothermal method and their electrocatalytic activities for hydrogen evolution reaction. *J Mater Chem*. 2010;20(9):1683-90.
7. Mourão HAJL, Lopes OF, Ribeiro C, Mastelaro VR. Rapid hydrothermal synthesis and pH-dependent photocatalysis of strontium titanate microspheres. *Materials Science in Semiconductor Processing*. 2015;30:651-7.
8. Ahmadian-Fard-Fini S, Ghanbari D, Salavati-Niasari M. Photoluminescence carbon dot as a sensor for detecting of *Pseudomonas aeruginosa* bacteria: Hydrothermal synthesis of magnetic hollow NiFe<sub>2</sub>O<sub>4</sub>-carbon dots nanocomposite material. *Composites Part B: Engineering*. 2019;161:564-77.
9. Ahmadian-Fard-Fini S, Salavati-Niasari M, Ghanbari D. Hydrothermal green synthesis of magnetic Fe<sub>3</sub>O<sub>4</sub>-carbon dots by lemon and grape fruit extracts and as a photoluminescence sensor for detecting of *E. coli* bacteria. *Spectrochimica Acta Part A: Molecular and Biomolecular Spectroscopy*. 2018;203:481-93.
10. Ahmadian-Fard-Fini S, Ghanbari D, Amiri O, Salavati-Niasari M. Electro-spinning of cellulose acetate nanofibers/Fe/carbon dot as photoluminescence sensor for mercury (II) and lead (II) ions. *Carbohydrate Polymers*. 2020;229:115428.
11. Moradi B, Nabiyouni G, Ghanbari D. Rapid photo-degra-



- dation of toxic dye pollutants: green synthesis of mono-disperse Fe<sub>3</sub>O<sub>4</sub>–CeO<sub>2</sub> nanocomposites in the presence of lemon extract. *Journal of Materials Science: Materials in Electronics*. 2018;29(13):11065-80.
12. Etminan M, Nabiyouni G, Ghanbari D. Preparation of tin ferrite–tin oxide by hydrothermal, precipitation and auto-combustion: photo-catalyst and magnetic nanocomposites for degradation of toxic azo-dyes. *Journal of Materials Science: Materials in Electronics*. 2017;29(3):1766-76.
  13. Kurian J, Mathew MJ. Structural, optical and magnetic studies of CuFe<sub>2</sub>O<sub>4</sub>, MgFe<sub>2</sub>O<sub>4</sub> and ZnFe<sub>2</sub>O<sub>4</sub> nanoparticles prepared by hydrothermal/solvothermal method. *Journal of Magnetism and Magnetic Materials*. 2018;451:121-30.
  14. Dong J, Wang Z, Kang X. The synthesis of graphene/PVDF composite binder and its application in high performance MnO<sub>2</sub> supercapacitors. *Colloids and Surfaces A: Physicochemical and Engineering Aspects*. 2016;489:282-8.
  15. Falahatgar SS, Ghodsi FE, Tepehan FZ, Tepehan GG, Turhan İ, Pishdadian S. Electrochromic performance of sol–gel derived amorphous MnO<sub>2</sub>–ZnO nanogranular composite thin films. *Journal of Non-Crystalline Solids*. 2015;427:1-9.
  16. Sun X, Gan M, Ma L, Wang H, Zhou T, Wang S, et al. Fabrication of PANI-coated honeycomb-like MnO<sub>2</sub> nanospheres with enhanced electrochemical performance for energy storage. *Electrochimica Acta*. 2015;180:977-82.
  17. Fei JB, Cui Y, Yan XH, Qi W, Yang Y, Wang KW, et al. Controlled Preparation of MnO<sub>2</sub> Hierarchical Hollow Nanostructures and Their Application in Water Treatment. *Advanced Materials*. 2008;20(3):452-6.
  18. Fan Z, Chen J, Wang M, Cui K, Zhou H, Kuang Y. Preparation and characterization of manganese oxide/CNT composites as supercapacitive materials. *Diamond and Related Materials*. 2006;15(9):1478-83.
  19. Rathinavel S, R D, Panda D, Manikandan A. Synthesis and characterization of MgFe<sub>2</sub>O<sub>4</sub> and MgFe<sub>2</sub>O<sub>4</sub>/rGO nanocomposites for the photocatalytic degradation of methylene blue. *Inorganic and Nano-Metal Chemistry*. 2020;51(2):210-7.
  20. Ansari SM, Ghosh KC, Devan RS, Sen D, Sastry PU, Kolekar YD, et al. Eco-Friendly Synthesis, Crystal Chemistry, and Magnetic Properties of Manganese-Substituted CoFe<sub>2</sub>O<sub>4</sub> Nanoparticles. *ACS Omega*. 2020;5(31):19315-30.
  21. Zhang N, Huang Y, Zong M, Ding X, Li S, Wang M. Synthesis of ZnS quantum dots and CoFe<sub>2</sub>O<sub>4</sub> nanoparticles co-loaded with graphene nanosheets as an efficient broad band EM wave absorber. *Chemical Engineering Journal*. 2017;308:214-21.
  22. Malinowska I, Rzyńska Z, Mrotek E, Klimczuk T, Zielińska-Jurek A. Synthesis of CoFe<sub>2</sub>O<sub>4</sub> Nanoparticles: The Effect of Ionic Strength, Concentration, and Precursor Type on Morphology and Magnetic Properties. *Journal of Nanomaterials*. 2020;2020:1-12.
  23. Kurian J, Jacob Mathew M. A facile approach to the elucidation of magnetic parameters of CuFe<sub>2</sub>O<sub>4</sub> nanoparticles synthesized by hydrothermal route. *Journal of Magnetism and Magnetic Materials*. 2017;428:204-12.
  24. M SP, A EP, S A. Development of multi-pass processed AA6082/SiCp surface composite using friction stir processing and its mechanical and tribology characterization. *Surface and Coatings Technology*. 2020;394:125900.
  25. Mazaheri Y, Karimzadeh F, Enayati MH. A novel technique for development of A356/Al<sub>2</sub>O<sub>3</sub> surface nanocomposite by friction stir processing. *Journal of Materials Processing Technology*. 2011;211(10):1614-9.
  26. Zayed EM, El-Tayeb NSM, Ahmed MMZ, Rashad RM. Development and Characterization of AA5083 Reinforced with SiC and Al<sub>2</sub>O<sub>3</sub> Particles by Friction Stir Processing. *Engineering Design Applications: Springer International Publishing*; 2018. p. 11-26.